Int. J. Electrochem. Sci., 12 **(2017)** 9925 – 9932, doi: 10.20964/2017.11.26

International Journal of
ELECTROCHEMICAL
SCIENCE
www.electrochemsci.org

Short communication

Integrated Charge Transfer in $Li_3V_2(PO_4)_3$/C for High-Power Li-Ion Batteries

Xianghua Zhang[1], *Dong Chen*[1], *Yipei Liu*[1], *Weiwei Han*[1], *Huaqiang Chu*[1,*], *Xianhong Rui*[1, 2,*]

[1]School of Energy and Environment, Anhui University of Technology, Maanshan, Anhui 243002, China
[2] Key Laboratory of Advanced Energy Materials Chemistry (Ministry of Education), Nankai University, Tianjin 300071, China
[*]E-mail: hqchust@163.com (H.Q. Chu), xhrui@outlook.com (X.H. Rui)

Received: 3 July 2017 / *Accepted:* 30 August 2017 / *Published:* 12 October 2017

To improve the charge transfer kinetics in monoclinic $Li_3V_2(PO_4)_3$ (LVP), LVP nanoparticles with sizes ranging from 100 to 200 nm that were completely encapsulated in amorphous carbon networks (LVP/C) are synthesized by a facile sol-gel method using two carbon sources of citric acid and span80 ($C_{24}H_{44}O_6$). Span80, possessing strongly hydrophilic functional groups, is essential for the formation of the three-dimensional conductive carbon matrix. When applied as the cathode for Li-ion batteries, LVP/C nanocomposite displays an excellent cycling stability and rate capability, e.g., delivering the capacity of 85 mAh g^{-1} at the high rate of 30 C.

Keywords: lithium ion battery, lithium vanadium phosphate, 3D carbon network, nanocomposite, high-power

1. INTRODUCTION

Due to the excessive use of fossil fuels and the emergence of various environmental problems, the development of renewable energies sources, such as solar, wind, and biomass energy, in order to replace traditional fossil fuels has become urgent. However, these renewable energies show the features of intermittent and uncertain power generation which limits their development, such that the development of energy storage technologies and capabilities for advanced renewable energy technologies are essential. As a representative energy storage technology, Li-ion batteries (LIBs) have become a heavily researched research topic in the renewable and sustainable energy developments, and great efforts have been devoted to develop new electrode materials for LIBs [1-5]. Monoclinic lithium vanadium phosphate $Li_3V_2(PO_4)_3$ (LVP) is generally considered to be an attractive candidate for the

positive electrode of rechargeable LIBs due to its high operating voltage, excellent rate performance, low-temperature operation, good thermal stability and safety [6, 7]. The three-dimensional (3D) framework of the monoclinic LVP structure is stabilized by the strong covalent bonds between the oxygen ions and the P^{5+} resulting in PO_4^{3-} tetrahedral polyanions. The large polyanion instead of the smaller O^{2-} in an open 3D framework not only helps to stabilize the structure but also enables fast ion migration[8, 9]. We note that the LVP contains three independent crystallographic lithium sites and all of these are mobile, yielding the high theoretical capacity of 197 mAh g^{-1} [10-12].

Unfortunately, similar to olivine-type cathodes, LVP also has the drawback of low electronic conductivity. Incorporation of carbon into LVP is a common approach to address this electronic limitation. This generally realized by introducing an organic precursor in the sample preparation procedure, that can be then converted into electronically conductive carbon through pyrolysis at high temperatures under inert atmospheres [13-16]. To date, there has been considerable research work on this hot topic of "coating a carbon film on the surface of LVP particles". For example, glucose and carbon nanotube (CNT) modified LVP exhibits the discharge capacity of 86.1 mAh g^{-1} at 10 C in the voltage range of 3.0 to 4.3 V [17]. A carbon-coated LVP cathode prepared by a low temperature solid-state route delivers the discharge capacity of 95.8 mAh g^{-1} at 10 C [18]. LVP/C particles electrode obtained by combination of spray-drying and carbothermal reaction using citric acid as carbon source displays the capacity of 61 mAh g^{-1} at 20 C rate in the range of 3.0-4.3 V [19]. LVP/C composite prepared on the basis of chelating reagents of glycine and beta-cyclodextrin releases a discharge capacity of 74.5 mAh g^{-1} at 50 C rate in the range of 3.0-4.3 V [20]. Furthermore, an LVP/graphene nanostructure exhibits the discharge capacity of 47 mAh g^{-1} at 50 C between 3.0 and 4.3 V [21]. Despite these successes, these composites show the common problem that the carbon coating is so uneven that some LVP particles are bare, leading to unsatisfactory rate performance, especially at rates of >10 C. The achievement of a fully carbon coated high-performance LVP by a facile method is still a great challenge.

In this study, we successfully synthesized LVP nanoparticles (100-200 nm) that completely are encapsulated in amorphous carbon networks by a simple sol-gel method using two carbon sources of citric acid (CA) and span80 ($C_{24}H_{44}O_6$). Span80 served as the additional carbon source to supplement the carbon layer obtained from citric acid in the LVP/C nanocomposite. It is noted that span80 has strongly hydrophilic functional groups that provide an orientation on the surface of the solution so that it is easier to form a 3D conductive carbon matrix for completely enclosing the LVP nanoparticles. As a result, the as-synthesized LVP/C nanocomposite demonstrates superior cycling stability and rate capability, e.g., delivering the capacity of 85 mAh g^{-1} at the high rate of 30 C.

2. EXPERIMENTAL

The LVP/C cathode materials were prepared by a sol-gel method using $CH_3COOLi{\cdot}2H_2O$, NH_4VO_3, $NH_4H_2PO_4$, citric acid ($C_6H_8O_7$) and span80 ($C_{24}H_{44}O_6$) as raw materials in the molar ratios of 3.00:2.00:3.00:2.40:0.35. In a typical synthesis, NH_4VO_3 was initially dissolved in distilled water under stirring at 60 °C, and then $CH_3COOLi{\cdot}2H_2O$ and $NH_4H_2PO_4$ were added to form a yellow

solution. Subsequently, citric acid and span80 were introduced and dissolved in the above solution with continuous stirring at 60 °C until a bright green gel was obtained. In this study, citric acid and span80 were employed as chelating reagents and carbon sources, giving rise to the cations and anions mixing at the molecular level. Meanwhile, they can be pyrolyzed to form the carbon network and coating carbon. Then, the precursor gel samples were ground and sintered at the temperature of 350 °C in a tubular furnace with flowing Ar/H_2 (5 vol%) gas for 4 h, followed by a re-sintering process for another 12 h at 750 °C in Ar/H_2 (5 vol%) atmosphere to yield the LVP/C nanocomposite.

The crystal structure was characterized by X-ray diffraction (XRD) using a diffractometer (Philips X'Pert Pro Super, Cu K_α radiation). The diffraction pattern was recorded at room temperature in the 2θ range from 10° to 60°. The surface morphology and nanostructure of the sample were observed by scanning electron microscopy (SEM, JSM-7500F) and transmission electron microscopy (TEM, JEM-2100F).

Coin-type cells were assembled for electrochemical measurements of the LVP/C cathodes. To prepare the cathodes for the testing, slurries of LVP/C nanocomposites, carbon black and poly (vinyl difluoride) (PVDF) in the weight ratio of 80:10:10 dissolved in N-methyl-2-pyrrolidone (NMP) were pasted on Al foils. The cells (CR2032 size) were fabricated in an argon-filled glove box with the LVP/C as the cathode, Li metal as the anode and 1 M solution of $LiPF_6$ in EC: DMC (1:1 w/w) as the electrolyte. The galvanostatic charge-discharge tests were conducted using a multi-channel battery test system (NEWARE BTS-610) in the voltage range of 3.0 to 4.3 V and 3.0 to 4.8 V.

3. RESULTS AND DISCUSSION

Fig. 1 shows the XRD pattern of the LVP/C nanocomposite synthesized by a sol-gel method with citric acid and span80 as the carbon sources. The sample can be identified as $Li_3V_2(PO_4)_3$ with the monoclinic structure (space group $P2_1/n$), in good agreement with the result reported previously [22-24]. The grain size, D, is calculated using the Scherrer's equation: $D=0.9\lambda/(\beta\cos\theta)$, where λ is the X-ray wavelength and β is the full-width-at-half-maximum of the diffraction peak on a 2θ scale.

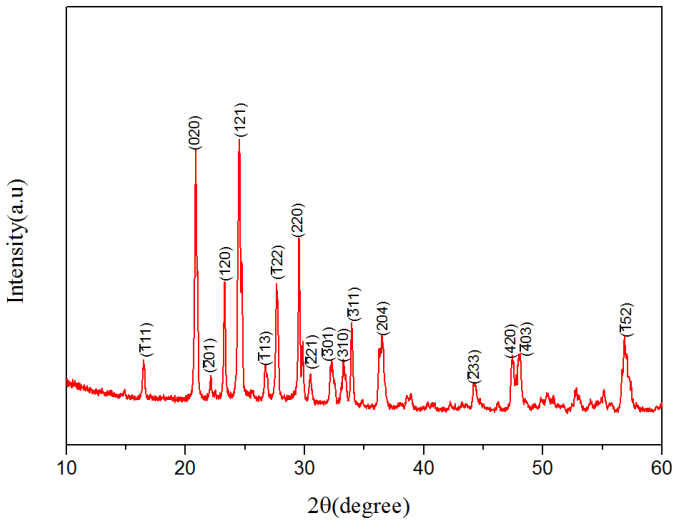

Figure 1. XRD pattern of the as-synthesized LVP/C nanocomposite.

Based on the (121), (020) and (220) diffraction peaks, *D* is found to be 41 nm, which is significantly smaller than that of the sample prepared by the solid-state reaction [7, 25-27]. In addition, the peaks related to carbon materials are not detected because the residual carbon is amorphous. Following the methodology of residual carbon measurement described in ref. [28], the residual carbon content in the LVP/C nanocomposite is calculated to be approximately 21 wt% based on its weight variation after the oxidation in air at 600 °C.

The surface morphology and nanostructure of LVP/C nanocomposite are displayed in Fig. 2. Examination of the SEM image presented in Fig. 2a shows that the LVP particles are uniformly dispersed in the carbon network and there are some pores with the sizes of several micrometers, which is beneficial for electron and lithium ion transport. TEM images (Figs. 2b and 2c) further verify that LVP nanoparticles with the sizes of 100-200 nm are completely encapsulated in amorphous carbon networks without exposure of any LVP nanoparticles. The particle size here is much smaller than that of LVP/C prepared using two carbon sources of phytic acid and oxalic acid (2.5 μm) [29] and sucrose-assisted LVP/C composite (500 nm) [30].

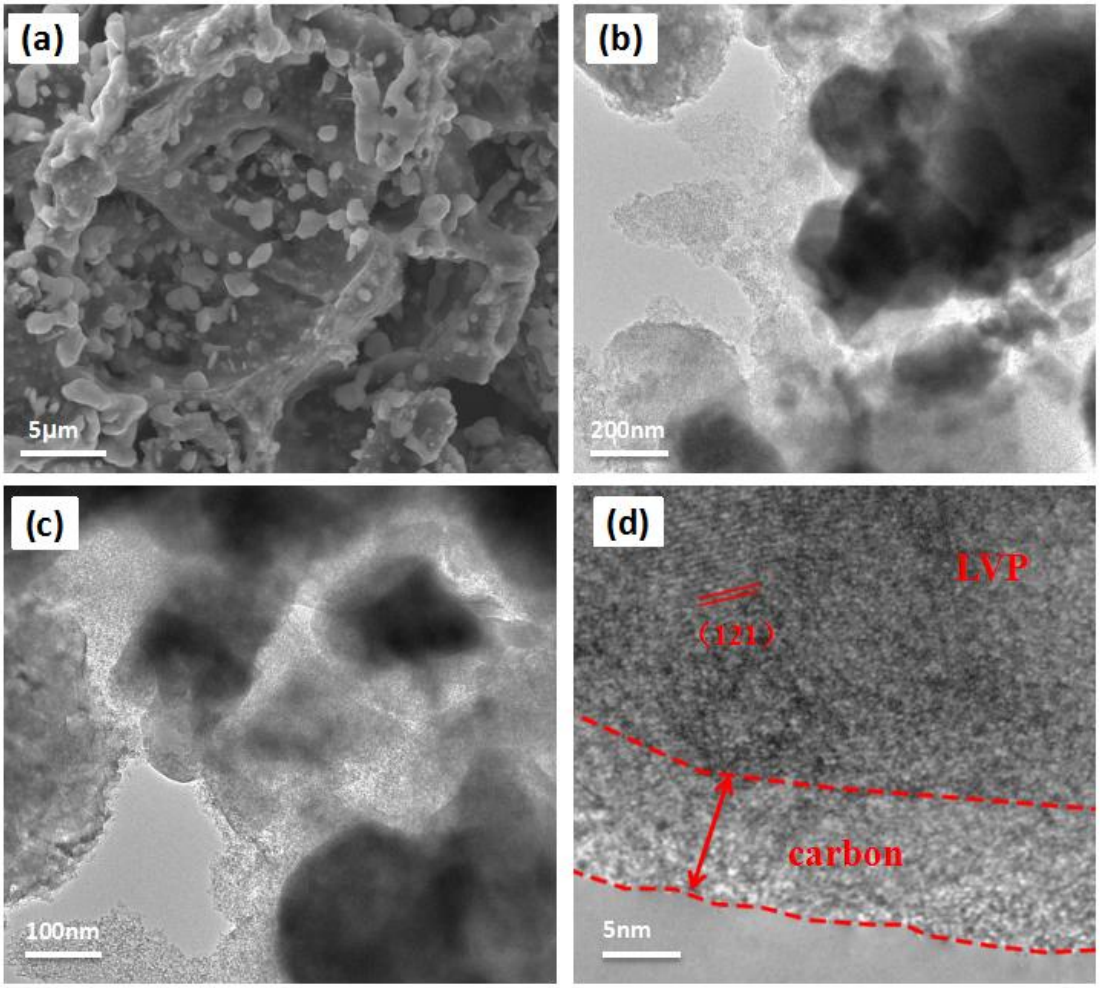

Figure 2. Morphology and nanostructure of LVP/C nanocomposite. (a) FESEM image, (b and c) TEM images, and (d) high-resolution TEM image.

Moreover, as indicated by the high-resolution TEM image (Fig. 2d), a uniform carbon layer (7 nm) coated on the surface of LVP nanoparticle is also present, which is thinner than that of the irregular carbon layer (10-20 nm) on LVP particles prepared using oxalic acid as the carbon source [31], and >10 nm carbon layer on oxalic acid and glucose-based LVP [32]. Thin carbon layer is beneficial for Li^+ transport. The lattice fringes with the spacing of 0.36 nm correspond to the (121) planes of the monoclinic LVP, further indicating the high crystallinity. These results demonstrated the presence of small nanoparticles, thin carbon coating layer, and carbon networks that are highly desirable for lithium diffusion and electronic conductivity.

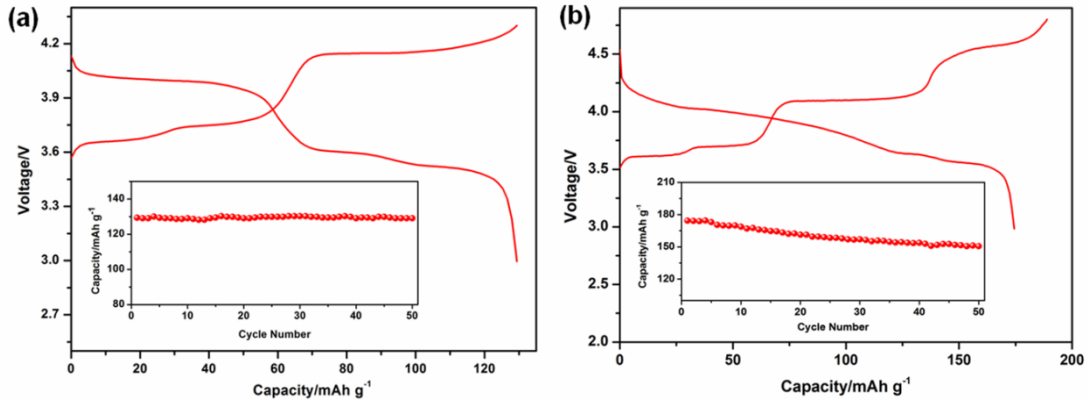

Figure 3. Initial charge-discharge curves and cycling performance (insets) of LVP/C nanocomposite at 0.5 C rate in voltage ranges of 3.0-4.3 V (a) and 3.0-4.8 V (b).

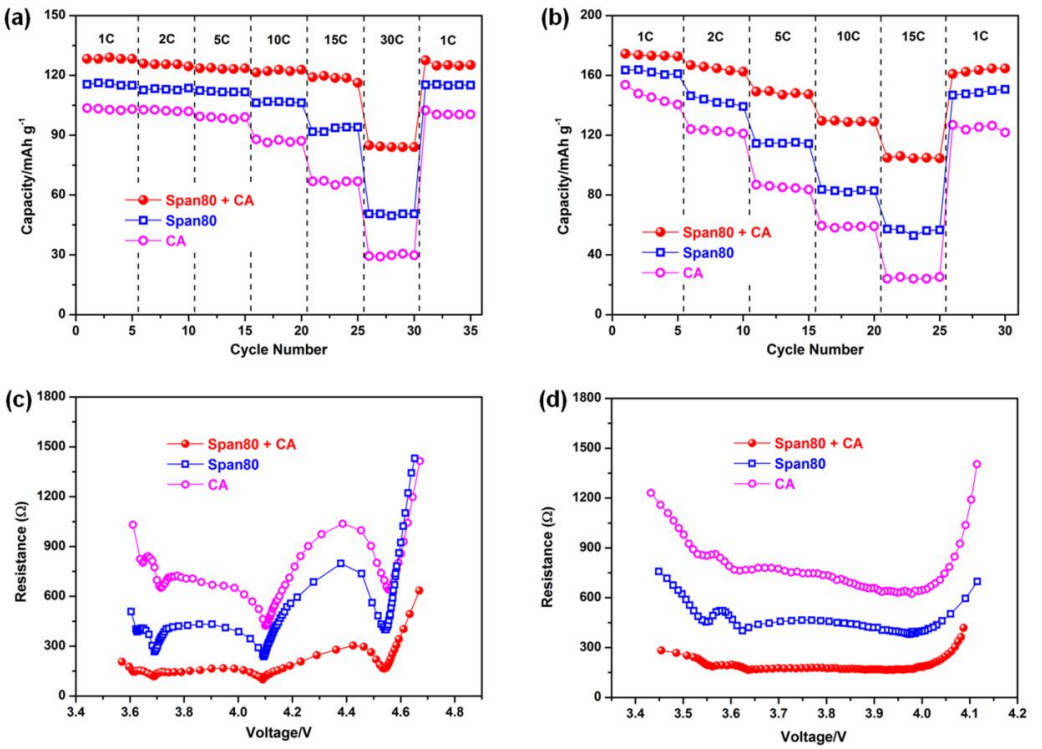

Figure 4. Rate performance of the as-synthesized LVP/C nanocomposite and reference LVP/C cathodes prepared with only CA and span80 in voltage ranges of 3.0-4.3 V (a) and 3.0-4.8 V (b); and their direct current resistance in voltage range of 3.0-4.8 V during charge (c) and discharge (d) processes.

The initial charge-discharge curves and cycling performance of the as-synthesized LVP/C at the rate of 0.5 C are illustrated in Fig. 3. In the voltage range of 3.0-4.3 V (Fig. 3a), there are three charge (3.65, 3.75 and 4.15 V) and discharge plateaus (3.50, 3.60 and 4.00 V), corresponding to two lithium extraction/insertion processes associated with the series of two-phase transitions of crystalline LVP, and the initial discharge capacity of 130 mAh g^{-1} is displayed. Such capacity is very close to the theoretical capacity, and higher than that of the LVP@C synthesized by a momentary freeze-drying method at 0.1 C (112 mAh g^{-1}) [33] and the polyamide-assisted LVP/C composite prepared by the carbon-thermal reduction method (125 mAh g^{-1}) [34]. Remarkably, an excellent capacity retention (i.e., no capacity fading) is demonstrated (inset in Fig. 3a). When charging to 4.8 V, the third lithium is extracted ($LiV_2(PO_4)_3 \rightarrow V_2(PO_4)_3$), and its associated initial charge-discharge profile and cycling performance are presented in Fig. 3b. The electrochemical discharge behavior is different from that in the voltage range of 3.0-4.3 V. It begins with a solid-solution behavior as indicated by the characteristic S-shaped curve, followed by two-phase transitions. As a result, the initial discharge capacity of 175 mAh g^{-1} (Coulombic efficiency: 87%) and an acceptable cycling stability (capacity retention: 86%) are achieved. When compared to previously reported LVP/C composites, e.g., 142 mAh g^{-1} at 0.5 C for LVP/C nanorods [35], 145 mAh g^{-1} at 1 C for LVP/C nanospheres [36] and 155 mAh g^{-1} at 0.5 C for microwave-assisted LVP/C [37], our capacity in voltage range of 3.0-4.8 V is also much enhanced.

The rate performance is shown in Fig. 4. To demonstrate the superiority of the as-synthesized LVP/C nanocomposite, the rate capabilities of the samples prepared with only one carbon sources (CA or span80) are also shown. It is clearly seen that the LVP/C nanocomposite prepared with both CA and span80 exhibits the best performance. In voltage range of 3.0-4.3 V (Fig. 4a), LVP/C nanocomposite shows discharge capacities of 129, 127, 124, 122 and 118 mAh g^{-1} at the rates of 1, 2, 5, 10 and 15 C, respectively. Even at the high rate of 30 C, the capacity of 85 mAh g^{-1} is still obtained. By contrast, the samples prepared with only CA and span80 display very low capacity values of 30 and 50 mAh g^{-1} at 30 C, respectively.

Table 1. A comparison of rate performance of the as-synthesized LVP/C nanocomposite with previously reported LVP/C composites.

Materials	Carbon sources	Rate performance	Ref.
LVP/C nanocomposite	citric acid and span80	118 (15 C) and 85 (30 C) mAh g^{-1} in 3.0-4.3 V 105 (15 C) mAh g^{-1} in 3.0-4.8 V	this work
LVP/C composite	chitosan	112 (15 C) mAh g^{-1} in 3.0-4.3 V	[38]
LVP/G	graphene	105 (15 C) mAh g^{-1} in 3.0-4.3 V	[21]
LVP@C composites	sucrose	110 (5 C) and 103 (10 C) mAh g^{-1} in 3.0-4.3 V	[13]
LVP@CMK-3	oxalic acid and CMK-3	95 (5 C) and 74 (10 C) mAh g^{-1} in 3.0-4.3 V	[12]
LVP/C nanoparticles	ethanolamine lactate	105 (5 C) and 96 (10 C) mAh g^{-1} in 3.0-4.3 V	[11]
LVP/C composite	citric acid	109 (5 C) mAh g^{-1} in 3.0-4.3 V	[39]

In the voltage range of 3.0-4.8 V (Fig. 4b), LVP/C nanocomposite shows discharge capacities of 173, 165, 148, 130 and 105 mAh g^{-1} at the rates of 1, 2, 5, 10 and 15 C, respectively. This performance is also much better than that of the two reference samples. On the other hand, it is important to mention that the capacity of LVP/C nanocomposite can be recovered to its initial values when the rate returns to 1 C, indicating that the structure does not collapse after high current charge-discharge processes. Furthermore, as compared to LVP/C composites in recent literatures (Table 1), the rate performance of our LVP/C nanocomposite is also excellent.

To understand the difference in the rate performance, the direct current (DC) resistance in the voltage range of 3.0 to 4.8 V was measured using the intermittent current interruption method [40]. As seen from Figs. 4c and 4d, there are four minimum peaks located at approximately 3.6, 3.7, 4.1 and 4.55 V during the charge process as well as three corresponding peaks at approximately 3.55, 3.62 and 4.0 V during the discharge process, agreeing well with the charge-discharge plateaus in Fig. 3b. It is also found that the LVP/C nanocomposite prepared with both CA and span80 demonstrates the smallest resistance values during both the charge and discharge processes, which is the reason why this cell can achieve the highest capacities at various C-rates.

4. CONCLUSIONS

The LVP/C nanocomposite was successfully synthesized by a sol-gel method using citric acid and span80 as the carbon sources. LVP nanoparticles (100-200 nm) are completely encapsulated in amorphous carbon networks, resulting in considerably enhanced charge transfer kinetics. When applied as the cathode for LIBs, the nanocomposite exhibits an outstanding electrochemical performance in terms of cycling stability and rate capability, e.g., delivering the capacity of 85 mAh g^{-1} at the high rate of 30 C.

ACKNOWLEDGMENTS
This work was supported by the National Science Foundation of China (No. 21606003 and 51676002), the Anhui Provincial Natural Science Foundation (No.1608085QB35), and the Opening Project of Key Laboratory of Advanced Energy Materials Chemistry (Chinese Ministry of Education).

References

1. B. Xu, D. Qian, Z. Wang, Y.S. Meng, *Mater. Sci. Eng*. R, 44 (2013) 51.
2. C. Liu, R. Massé, X. Nan, G. Cao, *Energy Storage Mater*., 4 (2016) 15.
3. L. Shen, Y.A. Liu, *Chem. Phys. Lett*., 677 (2017) 167.
4. S. Cavaliere, S. Subianto, I. Savych, D.J. Jones, J. Rozière, *Energy Environ. Sci.*, 4 (2011) 4761.
5. Y. Tang, Y. Zhang, W. Li, B. Ma, X. Chen, *Chem. Soc. Rev.*, 44 (2015) 5926.
6. X. Rui, Q. Yan, M. Skyllas-Kazacos, T.M. Lim, *J. Power Sources*, 258 (2014) 19.
7. K. Wu, J. Yang, *Mater. Res. Bull*., 48 (2013) 435.
8. L.L. Zhang, H.B. Sun, X.L. Yang, M. Li, Z. Li, S.B. Ni, H.C. Tao, *J. Solid State Electrochem*., 20

(2016) 311.
9. J. Xu, S.L. Chou, C. Zhou, Q.F. Gu, H.K. Liu, S.X. Dou, *J. Power Sources*, 246 (2014) 124.
10. S. Kim, J. Song, B. Sambandam, S. Kim, J. Jo, S. Park, S. Baek, J. Kim, *Mater. Today Commun*., 10 (2017) 105.
11. W. He, Q. Chen, T. Zhang, Y. Gao, *Micro Nano Lett*., 10 (2015) 67.
12. S. Wang, Z. Zhang, Z. Jiang, A. Deb, L. Yang, S.I. Hirano, *J. Power Sources*, 253 (2014) 294.
13. L. Zhang, L. Hu, L. Fei, J. Qi, Y. Hu, Y. Wang, H. Gu, *RSC Adv.*, 7 (2017) 25422.
14. Q. Zhang, S.K. Zhong, F.P. Li, *J. Power Sources*, 33 (2012) 213.
15. Z. Chen, H. Jin, C. Dai, G. Wu, M. Nelson, Y. Cheng, *Int. J. Electrochem. Sci*., 8 (2013) 8153.
16. Y.Q. Qiao, X.L. Wang, Y. Zhou, J.Y. Xiang, D. Zhang, S.J. Shi, J.P. Tu, *Electrochim. Acta,* 56 (2010) 510.
17. T. Lancet, *New J. Chem*., 39 (2015) 9617.
18. D. Tao, S. Wang, *J. Sol-Gel Sci. Techn*., 74 (2015) 121.
19. F. Yu, J. Zhang, Y. Yang, G. Song, *J. Solid State Electrochem*., 14 (2010) 883.
20. L. Wang, H. Liu, Z. Tang, L. Ma, X. Zhang, *J. Power Sources*, 204 (2012) 197.
21. H. Liu, G. Yang, X. Zhang, P. Gao, L. Wang, J. Fang, J. Pinto, X. Jiang, *J. Mater. Chem.*, 22 (2012) 11039.
22. X. Zhang, S. Han, C. Fan, *Ionics*, 21 (2015) 1509.
23. B.Q. Jiang, S.F. Hu, Z.Q. Ye, *Adv. Mater. Res*., 156-157 (2011) 1199.
24. L.L Zhang, Z. Li, X.L. Yang, X.K. Ding, Y.X. Zhou, H.B. Sun, H.C. Tao, L.Y. Xiong, Y.H. Huang, *Nano Energy,* 34 (2017) 111.
25. Q. Kuang, Y. Zhao, *J. Power Sources*, 216 (2012) 33.
26. L. Wang, X. Zhou, Y. Guo, *J. Power Sources*, 195 (2010) 2844.
27. G. Yang, H. Ji, H. Liu, B. Qian, X. Jiang, *Electrochim. Acta*, 55 (2010) 3669.
28. X.H. Rui, C. Li, J. Liu, T. Cheng, C.H. Chen, *Electrochim. Acta*, 55 (2010) 6761.
29. J. Su, X.L. Wu, J.S. Lee, J. Kim, Y.G. Guo, *J. Mater. Chem. A*, 1 (2013) 2508.
30. X. Min, H. Huo, R. Li, J. Zhou, Y. Hu, C. Dai, *J. Electroanal. Chem.*, 774 (2016) 76.
31. M.M. Ren, Z. Zhou, X.P. Gao, W.X.P. And, J.P. Wei, *J. Phys. Chem. C*, 112 (2008) 5689.
32. L.L. Zhang, Y. Li, G. Peng, Z.H. Wang, J. Ma, W.X. Zhang, X.L. Hu, Y.H. Huang, *J. Alloys. Compd.*, 513 (2012) 414.
33. C. Wang, H. Liu, W. Yang, *J. Mater. Chem.*, 22 (2012) 5281.
34. J. Yan, Y. Cao, F. Liu, *RSC. Adv.*, 6 (2016)113228.
35. H. Liu, C. Cheng, X. Huang, J. Li, *Electrochim. Acta*, 55 (2010) 8461.
36. L. Mai, S. Li, Y. Dong, Y. Zhao, Y. Luo, H. Xu, *Nanoscale*, 5 (2013) 4864.
37. B.Q. Jiang, S.F. Hu, M.W. Wang, *Adv. Mater. Res.*, 156-157 (2011) 1219.
38. W.F. Mao, J. Yan, H. Xie, Y. Wu, Z.Y. Tang, Q. Xu, *Mater. Res. Bull.*, 47 (2012) 4527.
39. F. Wang, F. Wu, C. Wu, Y. Bai, Z. Yang, *Adv. Mater. Res.*, 391-392 (2011) 1064.
40. X.H. Rui, C. Li, C.H. Chen, *Electrochim. Acta*, 54 (2009) 3374.